

# DiffFit: Visually-Guided Differentiable Fitting of Molecule Structures to Cryo-EM Map

Deng Luo , Zainab Alsuwaykit , Dawar Khan , Ondřej Strnád , Tobias Isenberg , and Ivan Viola 

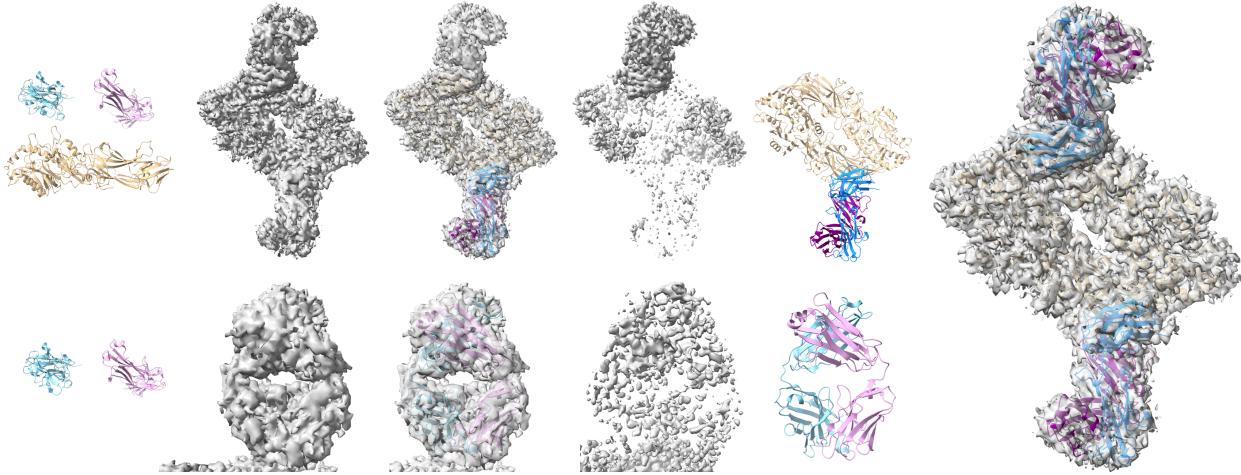


Fig. 1: Compositing a protein (PDB 8SMK [53]) from its three unique chains. Top row from left to right: three input chains, input target volume, the best fits in the first fitting round, the remaining voxels after *zeroing-out*, and the fitted chains. Bottom row from left to right: two remaining input chains, remaining region of interest in the target volume from the first round, the best fits in the second round, the remaining voxels after *zeroing-out*, the fitted chains. Right: the final composited structure overlaid on the original target volume. The involved computation takes 30 seconds in total, and the human-in-the-loop interaction takes  $\approx 5$  minutes.

**Abstract**—We introduce DiffFit, a differentiable algorithm for fitting protein atomistic structures into experimental reconstructed Cryo-Electron Microscopy (cryo-EM) volume map. This process is essential in structural biology to semi-automatically reconstruct large meso-scale models of complex protein assemblies and complete cellular structures that are based on measured cryo-EM data. Current approaches require manual fitting in 3D that already results in approximately aligned structures followed by an automated fine-tuning of the alignment. With our DiffFit approach, we enable domain scientists to automatically fit new structures and visualize the fitting results for inspection and interactive revision. Our fitting begins with differentiable 3D rigid transformations of the protein atom coordinates, followed by sampling the density values at its atom coordinates from the target cryo-EM volume. To ensure a meaningful correlation between the sampled densities and the protein structure, we propose a novel loss function based on a multi-resolution volume-array approach and the exploitation of the negative space. Such loss function serves as a critical metric for assessing the fitting quality, ensuring both fitting accuracy and improved visualization of the results. We assessed the placement quality of DiffFit with several large, realistic datasets and found its quality to be superior to that of previous methods. We further evaluated our method in two use cases. First, we demonstrate its use in the process of automating the integration of known composite structures into larger protein complexes. Second, we show that it facilitates the fitting of predicted protein domains into volume densities to aid researchers in the identification of unknown proteins. We implemented our algorithm as an open-source plugin ([github.com/nanovis/DiffFitViewer](https://github.com/nanovis/DiffFitViewer)) in ChimeraX, a leading visualization software in the field. All supplemental materials are available at [osf.io/5tx4q](https://osf.io/5tx4q).

**Index Terms**—Scalar field data, algorithms, application-motivated visualization, process/workflow design, life sciences, health, medicine, biology, structural biology, bioinformatics, genomics, cryo-EM.

## 1 INTRODUCTION

As humans we have been striving for centuries and even millennia to understand, as Faust says, “*was die Welt im Innersten zusammenhält*

[what binds the world, and guides its course]” [46]. This quest applies, among other directions of scientific inquiry, to the inner working of the biological world. In particular, we are trying to understand how the biological processes at tiny scales work and how they, ultimately, keep us alive. In the field of structural biology, traditionally we have relied on techniques such as X-ray crystallography or nuclear magnetic resonance spectroscopy to understand the actual molecular compositions of cells and organelles—yet with the limitation that these could only provide (still impressive and highly useful) estimates or manually constructed models of the structure of actual biological samples (e.g., [5, 22, 30, 37, 42, 45]). In the recent few years, however, the Cryo-Electron Microscopy (cryo-EM) approach [29] has opened the doors to visualizing the biomolecules within *actual samples* at near-atomic resolution. In addition, the Protein Data Bank (PDB) initiative has over decades collected thousands of molecular models of the building blocks of the cells or organelles studied in structural biology. This

• Deng Luo (罗登), Zainab Alsuwaykit (زینب السویک), Dawar Khan (دوار خان), Ondřej Strnád, and Ivan Viola are with the Visual Computing Center at King Abdullah University of Science and Technology (KAUST), Saudi Arabia. E-mail: {deng.luo | zainab.alsuwaykit | dawar.khan | ondrej.strnad | ivan.viola}@kaust.edu.sa.

• Tobias Isenberg is with Université Paris-Saclay, CNRS, Inria, LISN, France. E-mail: tobias.isenberg@inria.fr.

Manuscript received xx xxx. 202x; accepted xx xxx. 202x. Date of Publication xx xxx. 202x; date of current version xx xxx. 202x. For information on obtaining reprints of this article, please send e-mail to: [reprints@ieee.org](mailto:reprints@ieee.org). Digital Object Identifier: [xx.xxxx/TVCG.202x.xxxxxxx](https://doi.org/10.1109/TVCG.202x.3000000)

new situation means that we are now at the brink of reconstructing the molecular composition of actual samples at a ground-truth level.

Yet to achieve this type of reconstruction we not only need to interactively visualize molecular data, for which tools [41] exist, but need to be able to faithfully place 3D models of known molecular building blocks, such as from PDB data and the AlphaFold predicted library [17], to the captured cryo-EM datasets. So far, the fitting process involves a substantial time commitment and numerous manual interventions by the domain experts—rendering this process not very effective. The sheer complexity and size of the involved molecules, combined with the variability and noise inherent in cryo-EM data, pose substantial obstacles. A fully automatic process, in contrast, is also not the ideal solution because the existence of local minima (wrong placement of the compositing proteins) requires the domain experts to verify each placement where they utilize their knowledge and experience. Fully automated methods are currently far from feasible. Instead, we need the optimal balance between user interaction and automation.

For this purpose, we developed DiffFit, an automated differentiable fitting algorithm coupled with visual inspection and decision making, designed to optimize alignment between protein structures and experimental reconstructions of volumes (i. e., cryo-EM maps). Our technique works in both one-to-one fitting scenarios and many-to-one scenarios, in which multiple protein subunit structures are precisely aligned with a single, large, experimentally reconstructed volume. The DiffFit method is iterative and gradually brings the source protein structures into the target volumes to stepwise reconstruct the molecular-subunits alignment. By leveraging advanced strategies such as volume filtering, multi-resolution volumes, and negative space utilization, we construct a loss function that allows us to quantify the fitting accuracy both during the iterations and for the final decision making. In this way we iteratively reduce the differences between the two representations—volumetric and atomistic—until we achieve the desired fit. Through this visually-guided fitting procedure we thus relieve the domain experts from manually placing structures as they assemble the reconstruction of the cryo-EM map, thus significantly speeding up the process into a manageable interactive procedure, that yields results at sufficient precision for the visualization and analysis of complex, real-world protein structures, ultimately facilitating large-scale structural modeling initiatives. In summary, we contribute:

- a differentiable fitting algorithm designed to fit multiple molecular subunits to a single reconstructed cryo-EM volume;
- human-in-the-loop strategy providing visual inspection and decision-making within an iterative structure-discovery cycle;
- a novel loss function and data processing that calculates new updates in each iteration to expedite algorithm convergence and quantify fitting accuracy; and
- three use-case scenarios of fitting either one or multiple known subunits or identifying yet unknown subunits being part of the molecular assembly.

## 2 BACKGROUND AND RELATED WORK

We rely on cryo-EM data, so below we first briefly provide essential relevant background. Then we describe past work on image registration and model fitting and show how both relate to our own research.

### 2.1 Brief background

Structural biology employs various techniques to understand how atoms are arranged in macromolecular complexes, i. e., samples in the range of 60 kDa (i. e., 4,472 atoms; [PDB 6NBD](#) [14]) to 50,000 kDa (3,163,608 atoms; [PDB 8J07](#) [47]) that are essential for scientists to study processes in living cells—cryo-EM being a particularly powerful one [2, 23, 25]. With cryo-EM, bioscientists capture images using an electron microscope of flash-frozen biological specimens, preserving their natural structure without any staining or fixing [3], which would otherwise interfere with the sample. These images are then used to construct cryo-EM 3D volumes or maps using the so-called *single particle method* that aligns thousands of projections from structurally identical molecular instances into a single map (using the Fourier slice-projection theorem)

representing the electron density of the sample, which can be used to infer the atom positions within the molecule.

Subsequently, the bioscientists need to build accurate atomistic or molecular models that match the electron density map obtained from the cryo-EM process to gain insight into molecular function and interactions. This process involves mapping or fitting known sub-molecules into their corresponding positions within the map. The objective is to achieve an optimal correspondence between the model and the experimental or simulated volume, revealing the organization of molecules in 3D space, including single molecules, complexes, and the placement of small molecules and ligands into binding sites. Molecular models are available in the Protein Data Bank (PDB, [rcsb.org](#)), accessible in various formats such as PDB, Crystallographic Information File (CIF), and mmCIF (macromolecular CIF). The fitting itself is today typically achieved through manual placement, alignment, and comparison with the density maps. The manual character of this process makes it extremely time-consuming and tedious, and means that only expert biologists can complete it. To address this challenge, numerous studies have aimed to automate the fitting process, focusing on image registration as the foundation and exploring methods to streamline 3D model construction as we review below.

### 2.2 Image registration and geometric fitting

The fitting of 3D structures into captured or simulated volumes relates to the problem of image registration in image processing. It entails aligning two images within a shared reference frame, regardless of whether they originate from the same or different modalities [8, 15]. This process involves feature extraction, determining transformations, and assessing accuracy through metrics. Scale-invariant features from images [24], for example, can facilitate matching across diverse views, despite significant distortions or variations. This process involves detecting invariant keypoints using the difference-of-Gaussian function, determining locations and scales, assigning directions based on local gradients, and measuring gradients within selected scales around each keypoint. Extracted features are stored in a database and can then be matched with new images using fast nearest-neighbor algorithms, with applications including object recognition. Among many applications of the process, physicians rely on various imaging modalities to diagnose patients, each capturing images with differing orientation. Image registration addresses this variability by aligning images within a unified frame by optimizing parameters like orientation and translation. Medical image registration is an active research area which encompasses diverse methods, including techniques based on cross-correlation [4, 26] and those based on mutual information [20, 28, 33, 44]. Shang *et al.* [40], e.g., introduced a method for medical image registration using principal component analysis (PCA) neural networks to extract feature images and compute rotation angles and translation parameters by aligning the first principal directions and centroids in a simple and efficient way. For complex spatial transformations, another recent approach [1] uses Kernel PCA and Teaching-Learning-based optimization (TLBO) for multi-modal image registration. Similar to these methods, transformations and alignments need to be determined to fit the atomistic model into a volumetric map. We can thus also use optimization techniques in cryo-EM map fitting to refine the fit and optimize parameters such as orientation and translation—which is what we show with our work. The major difference to image registration is that, in our workflow, we fit two different data representations and one is a sub-part of the whole that is potentially present at multiple locations in the target volume.

The model-to-data fitting that we need for cryo-EM data is a problem that has also been investigated in depth in computer graphics and pattern recognition [18, 35]. It has applications not only in structural biology but is also needed in architectural geometry, virtual and augmented reality, robotics, and various other fields [6, 21, 38, 52]. The key challenges in geometric fitting include accuracy, efficiency, robustness, and usability of the fitting module [21, 38]. Structural biology, in contrast, has special challenges such as noisy data, non-geometric shapes, and large data sizes so that geometric fitting methods are not directly applicable.

Yet our DiffFit algorithm still relates to techniques from computer graphics and pattern analysis. The differentiable compositing technique

proposed by Reddy *et al.* [35], in particular, offers valuable insights into addressing fitting challenges as well as manipulating and understanding image patterns. With *differentiable compositing* we can handle patterns effectively, outperforming state-of-the-art alternatives in pattern manipulation [39, 54]. Reddy *et al.*'s method [35] discovers complex patterns by aligning elements with their own position and rotation, and facilitates refinement based on similarity to the target for precise adjustment. In addition, Reddy *et al.* use a multi-resolution pyramid—relevant for handling the multi-resolution volumetric data in our domain. Reddy *et al.*'s method [35], however, is restricted to certain pattern types, requires manual element marking, and may not always find the best solution, leading to orientation errors and missed elements. Nevertheless, we build our solution on top of their differentiable compositing.

Another approach, spline surface fitting [38], enhances the smoothness in aircraft engine geometry reconstruction by concurrently approximating point and normal data, ensuring boundary smoothness and optimal convergence, while exploring norm-like functions' effects on error measurement. A further recently proposed adaptive spline surface fitting method [21] employs surface meshes for high-precision CAD applications, supported by empirical evidence. The reliance on control meshes of this approach, however, limits its applicability to irregular topologies and compromise the preservation of sharp features. All these methods have common objectives and tasks such as similarity measures, pattern matching, fitting, and geometric transformations and, thus, can serve as a motivation and starting point toward our goals in structural biology. Since structural biology data often consists of large, complex structures without regular shapes like CAD models or easy representations in geometric meshes with smooth surfaces, however, the aforementioned methods are not directly applicable to our data.

### 2.3 Fitting in structural biology

Existing fitting methods for structural biology can roughly be categorized into manual, semi-automated, and automated approaches, each with its own advantages and challenges when used for aligning molecular models with cryo-EM density maps. Manual or semi-automated methods naturally involve human intervention, yet they provide control and precision—which is particularly beneficial in the structural analysis of complex datasets or when specific adjustments are needed for accuracy. For example, a popular tool for molecular manipulation and visualization, UCSF ChimeraX [31], includes the *fitmap* technique [11]. It suggests multiple possible placements of the atomistic model on the density map and then asks the user to make the final decision. The fitting process alternates between rigid-body rotation and gradient descent translation. In this way it maximizes the alignment between the atomic model and the density data by optimizing the sum of density values. Nonetheless, all of these manual or semi-automatic approaches are time-consuming and require a significant level of expertise.

To tackle this challenge and to automate the fitting process, researchers have developed methods that rely on deep learning (DL) [43, 50, 51].  $A^2$ -Net by Xu *et al.* [51], for example, uses DL to accurately determine amino acids within a 3D cryo-EM density volume. It employs a sequence-guided Monte Carlo Tree Search (MCTS) to traverse candidate amino acids, considering the sequential nature of amino acids in a protein. Here, the authors divide the problem of molecular structure determination into three subproblems: amino acid detection in the density volumes, assignment of atomic coordinates to determine the position of each amino acid, and main chain threading to resolve the sequential order of amino acids that form each protein chain. Xu *et al.*'s method also demonstrates a remarkable speed improvement, being 100 times faster in finding solutions at runtime than existing methods [7, 49], while achieving an excellent accuracy of 89.8%. In addition, they introduced the  $A^2$  dataset with 250,000 amino acids in 1,713 cryo-EM density volumes, with a resolution of  $3\text{ \AA}^\circ$ , pioneering automated molecular structure determination training benchmarks.

Another recent method by Mallet *et al.* [27] for finding antibodies in cryo-EM densities CrAI uses machine learning (ML). They formulate the objective as an object detection problem, using the structural properties of Fabs (Fragment antigen-binding) and VHJs (single-domain antibodies). Furthermore, DeepTracer [32] is a fully automated DL-

based method designed to determine the all-atom structure of a protein complex using its high-resolution cryo-EM map and amino acid sequence. It employs a customized deep convolutional neural network primarily for precise prediction of the protein structure, including the locations of amino acids, backbone, secondary structure positions, and amino acid types. The reprocessed cryo-EM maps are the input to the neural network, which transforms the output into a protein structure. Despite yielding accurate outcomes, the resulting atomistic structures may exhibit geometric issues, local fit to map discrepancies, misplaced side chains, or errors in tracing and/or connectivity. All DL-based techniques, moreover, not only require a substantial amount of time for the training (as opposed to the runtime) but also rely on large training datasets of cryo-EM volumes and manually fitted sub-molecules—which is why we do not resort to DL approaches.

An alternative to DL is map-to-map alignment, which is used to accurately align two-dimensional or three-dimensional maps to facilitate comparison and analysis of spatial structures or features within the maps. CryoAlign [13] is a cryo-EM density map alignment method that achieves fast, accurate, and robust comparison of two density maps based on local spatial feature descriptors. This approach involves sampling the density map to generate a point cloud representation and extracting key points by clustering based on local properties. CryoAlign then calculates local feature descriptors to capture structural characteristics, reducing the number of points considered and improving efficiency. By employing a mutual feature-matching strategy, CryoAlign establishes correspondences between keypoints in different maps and uses iterative refinement to enhance alignment. A combination of fast rotational matching search based on spherical harmonics and translational scans [10] yields accurate fitting results in seconds to a few minutes. This ADP\_EM approach is reliable, in particular, for fitting X-ray crystal structures to low-resolution density maps, with reduced docking times and while maintaining a thorough 6D exploration with fine rotational sampling steps to find valid docking solutions.

In our work, we design a differentiable optimization method for fitting atomistic structures into volumetric data with the goal of precise fitting with fast-enough computation to be applicable in semi-automatic fitting in the standard tool ChimeraX. For this purpose we make use of the PyTorch capabilities for GPU parallel computing, trilinear interpolation sampling in volumetric data, and auto differentiation.

## 3 METHOD

We begin to describe our approach by explaining our process of differentiable structure fitting, before we show how it can be used for visually-guided fitting. After discussing these conceptual aspects, we also briefly discuss implementation details.

### 3.1 Differentiable structure fitting

Given a cryo-EM map, the domain practitioners—bioscientists—do not know the precise location and orientation parameters that govern where and how a protein's sub-structures fit together. For some regions in the map, the bioscientists may not even know which protein subunits are supposed to be present. Our goal is to develop a new approach that addresses both of these domain tasks. For certain protein subunits, bioscientist are highly confident about their presence in the map. In such cases, our technique will aid in the identification of their respective placement parameters. Second, for the regions with unknown protein subunits, the task of our technique is to identify potential protein subunit candidates from a large database that best fit the cryo-EM map region.

#### 3.1.1 Inspiration and approach overview

We base our approach on the previously mentioned 2D differentiable compositing approach by Reddy *et al.* [35], which discovers pattern structure from wallpaper-like textures containing repetitive patterns made out of elementary patches. We first review their approach, before we describe how we build up our solution on top of their technique. In their case, given a 2D image, which is a composite of multiple small element patches, the task is to identify the number of occurrences of each patch and the placement parameters for each existing patch. The parameters include the type of patch out of several known patches

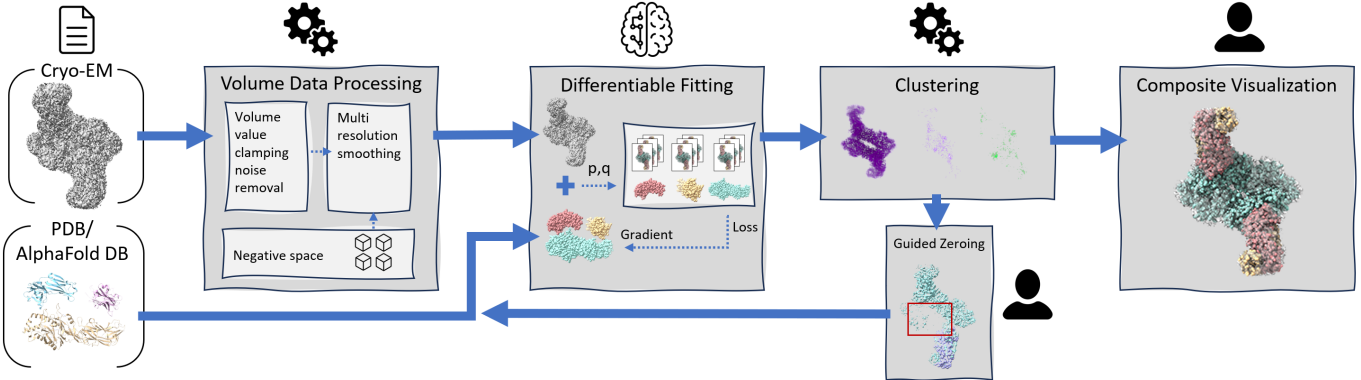


Fig. 2: DiffFit workflow. The target cryo-EM volume and the structures to be fit on the very left serve as inputs, which are passed into the novel volume processing, followed by the differentiable fitting algorithm. The fitting results are then clustered and inspected by the expert. The expert may zero out voxels corresponding to the placed structures and feed the map back iteratively as input for a new fitting, round until the compositing is done.

as well as position, orientation, and depth. Their solution distributes tens to hundreds of patches in the image and uses the differentiable optimization methodology to translate and reorient patterns such that they correspond to the appearance of the patterns in the input wallpaper image. Each single instance  $E_i$  (out of total number of  $\omega$  instances) of a pattern is stored in a layer  $J_i$  for each patch instance by sampling from that patch, with the translation, rotation, and patch-pattern type probability taken into account:

$$J_i(\mathbf{x}) = f_t(\mathbf{x}, E_i) = \frac{1}{\sum_{k=1}^{\omega} e^{t^k}} \sum_{j=1}^{\omega} e^{t^j} h_j \left( R_{\theta_i}^{-1} (\mathbf{x} - \mathbf{c}_i) \right) \quad (1)$$

where  $f_t(\mathbf{x}, E_i)$  is a differentiable function using the expected value over patch-pattern type probabilities stored in a tuple  $t$  representing all  $\omega$  patch patterns; softmax  $e^{t^k} / \sum_{k=1}^{\omega} e^{t^k}$  over type logits define the patch-pattern type probabilities;  $h_j$  is the image patch sampler function;  $\mathbf{x}$  is the image location;  $\mathbf{c}_i$  is center location of patch element  $E_i$ ; and  $R_{\theta_i}^{-1}$  is the inverse of a  $2 \times 2$  matrix rotation with angle  $\theta_i$ .

The solution image results from compositing of all instances together using  $f_c$  compositing function so that each known patch-pattern type is present multiple times with various positional parameters. Patches can overlap other patches, which leads to partial or full occlusion of a certain pattern. This is characterized by  $v_i(\mathbf{x}), v \in \{0, 1\}$ , which is the visibility of layer  $i$  at image location  $\mathbf{x}$ :

$$I(\mathbf{x}) = f_c(\{J_i(\mathbf{x})\}_i) = \sum_{i=0}^{\omega} J_i(\mathbf{x}) v_i(\mathbf{x}) \quad (2)$$

This solution image is compared with the input image in an optimization, where the parameters of all patch instances are updated in every iteration. The solution image then becomes increasingly similar to the input image. Reddy *et al.* define the  $L^2$  distance loss  $L_d$  for the optimizer as:

$$L_d(A, I) = \frac{1}{P} \sum_{p=1}^P \|A(\mathbf{x}_p) - I(\mathbf{x}_p)\|_2^2 \quad (3)$$

where the sum is over the number of all pixels  $P$  in the image.  $A$  is the input image and  $I$  is the composited solution image. The optimal elements  $\mathcal{E}^*$  are then found by minimizing loss  $L_d$  over the entire set of elements  $\mathcal{E} = \{E_0, \dots, E_\omega\}$ :

$$\mathcal{E}^* = \arg \min_{\mathcal{E}} L_d(A, f_c(\mathcal{E})). \quad (4)$$

Reddy *et al.*'s patch-pattern fitting problem is similar to ours in the sense that in both cases we are compositing element instances into a scene. But Reddy *et al.*'s differentiable compositing approach cannot be directly applied to the structural biology domain to solve the protein fitting problem for the following reasons:

1. the pattern image and the element patches are defined in 2D with layers, while the cryo-EM map and protein subunits are defined in 3D;
2. the pattern image and the element patches are of the same representation, i.e., 2D grid data, while the cryo-EM map and protein subunits are of different representations—one is a 3D volume while the other is a set of atom coordinates that can be regarded as a point cloud;
3. the instance patches in differentiable compositing are all of the same size, while the protein subunits differ in numbers of atoms;
4. differentiable compositing expects the patches to overlap, while protein subunits do not spatially overlap; and
5. forming 1000 layers of 2D images is possible to fit into the current GPU memory, while forming 1000 3D volumes is prohibitive with the currently available GPU memory.

Initially, we attempted to align our problem better with differentiable compositing by first *simulating* a cryo-EM map from the atomistic point cloud of the protein model and then fitting the simulated map to a target map. That way the representational discrepancy (see reason (2) above) is eliminated. That approach, however, was only successful for trivial cases, while for real-world scenarios it frequently fell into local minima. Interested reader will find exemplary volume-only based molecular fitting videos in supplementary material at [osf.io/5tx4q/](https://osf.io/5tx4q/).

Driven by the successful fitting cases from many experiments, we gradually built several novel strategies on top of differentiable compositing that effectively address the problem of molecular structure fitting. Most notably, we address the substantially higher complexity of our scenario based on the knowledge, experience, and deep insight of the target audience: the bioscientists. Our solution is thus based on a human-in-the-loop strategy and we propose a fast and robust visual analytics approach, DiffFit, with two main steps: (1) an automated excessive molecular fitting and (2) a visual inspection and filtering of the fitted results by bioscientists. These two consecutive steps are building blocks of a visual analytics feedback loop, in which multiple proteins are iteratively composited to fit the underlying cryo-EM volume.

We schematically present our DiffFit workflow in Fig. 2. First, we seed an excess amount of all compositing molecules in the volume scene. If fitting all molecules simultaneously exceeds the available GPU memory, we sort the molecules by atom count and partition them into batches. Then, we fit the batches of molecules within several iterations in descending atom-count order. For this fitting we rely on a novel loss function that calculates the average density value from densities at each atom. The differentiable property of our fitting scenario allows us to use optimization based on gradient-descent. In addition, we associate each fit with a numerical value that characterizes the quality of fit. For this purpose, we create a simulated cryo-EM map of each fitted molecule and calculate the correlation of the simulated densities with the real cryo-EM map densities. Then, we collect the fitting results and cluster them based on positional and orientational parameters. For each cluster,

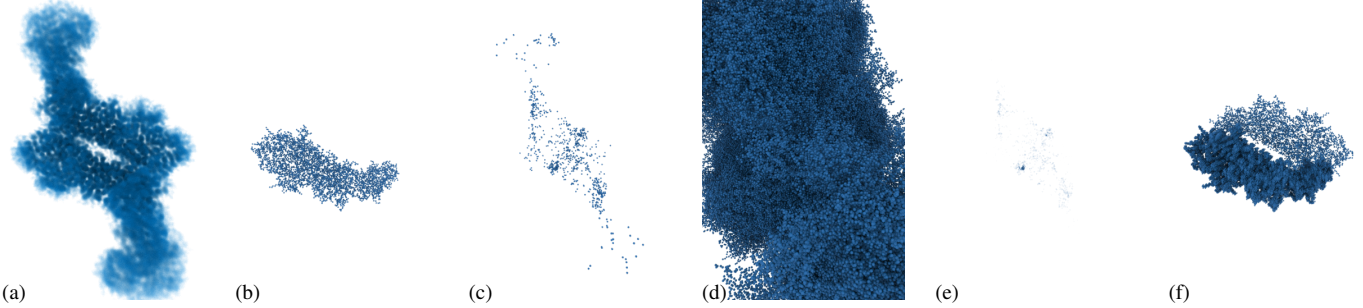


Fig. 3: Clustering and filtering: (a) target volume, (b) atom coordinates of the source structure, (c) positions of 1000 fit results (the dots are clustered, hiding the number of results), (d) 1000 instances of the structure, (e) positions of 1000 fit results with a transparency level set based on an exponential scaling of the correlation metric (two clusters stand out), and (f) instances of the structure at those two clusters.

we select one representative fit—the fit with the highest correlation value. We then sort the clusters by their representatives’ correlation and interactively visualize them in ChimeraX to allow the bioscientists to inspect the solutions. Once a given molecular placement is verified, we disable molecule placements in the respective regions in the following iterations by setting the those voxels in the cryo-EM map volume to zero that are covered by the molecular fit. We thus gradually erase the successful placements from the map, forcing following placements to search for a fit in non-zero volume locations. Once the feedback update in the map is completed, we perform the next iteration of fitting with another molecular structure. We repeat this workflow pattern until the map has nearly all voxels zeroed out and the entire sub-unit placement of the complex molecular structure is complete. Below we introduce the details of DiffFit, in the following order: (1) sample one coordinate; (2) fit one placement of one molecule; (3) fit multiple placements of one molecule; and (4) fit multiple placements of multiple molecules.

### 3.1.2 Sampling of one coordinate

Because our task is to find the optimal alignment of an atomistic molecular structure to the reconstructed cryo-EM volume map, we are searching for the optimal fit characterized by two rigid-body transformation parameters: a translational offset  $\mathbf{p}$  and a rotation. The rotation is represented by a quaternion  $\mathbf{q}$  or its corresponding rotation matrix  $M_{\mathbf{q}}$ . The position  $\mathbf{x}_i$  corresponds to the center point of an atom  $i$  within the molecular subunit for which we are finding the fit. For the calculation of the fit, we transform every atom position in one subunit according to the rotation and translational offset:

$$T(\mathbf{x}_i) = M_{\mathbf{q}} \cdot \mathbf{x}_i + \mathbf{p}$$

We sample a density value  $D$  of the atom to be placed at position  $T(\mathbf{x}_i)$  from a scalar volume  $V$  by trilinear interpolation as:

$$D(T(\mathbf{x}_i)) = S(T(\mathbf{x}_i), V)$$

### 3.1.3 Placement of one molecule (or one subunit)

To find the best  $\mathbf{p}$  and  $\mathbf{q}$  parameters we formulate an initial loss function  $L$  that gives us the minimum negative average density per atom for a molecular subunit with  $N$  atoms that form the set  $\mathbf{X}_m$  of all atom center points  $T(\mathbf{x}_i) \in \mathbf{X}_m$  for a particular molecular subunit  $m$ :

$$L(\mathbf{p}, \mathbf{q}, \mathbf{X}_m, V) = - \left( \frac{1}{N} \sum_i^N D(T(\mathbf{x}_i)) \right) = - \frac{1}{N} \sum_i^N S(M_{\mathbf{q}} \cdot \mathbf{x}_i + \mathbf{p}, V). \quad (5)$$

For the optimization we rely on the calculation of the gradient of our differentiable formulation and use it with the Adam optimizer [19]. Despite the Adam optimizer being known for robustness with respect to local minima, our initial loss function formulation frequently led to such a local minimum, i.e., a place that is not an optimal placement of the molecule in the map but from which the optimizer cannot find better solution in the parameter-space neighborhood. Such local minima are a common and severe problem that is also manifested in the functionality of most commonly used tools for molecular subunit fitting (e.g.,

ChimeraX’s fit-in-map feature). We thus introduced several strategies to form a novel loss function and, ultimately, make DiffFit more robust.

A first strategy that we found to substantially contribute to a good fitting performance is **filtering of the input cryo-EM map volume  $V$** . For this purpose we clamp the volume values based on a user-specified minimal threshold and a minimum size of connected-voxels that form a cluster. We also detect all voxels with a density value smaller than a given threshold and set them to zero. The size of the connected voxel cluster after thresholding has to be bigger than the cluster size hyperparameter. Otherwise, we set all the voxels in that cluster to zero. This step leads to the filtered volume  $V_F$  and ensures that only relevant volume regions are considered for fitting, improving the algorithm’s focus and efficiency. We then normalize the filtered values to  $[0, 1]$ —a typical practice in learning and optimization approaches—which leads to a volume  $\hat{V}_F$  and which turns out to be essential for controlling the magnitude of the calculations that lead to the loss function and hence the settings of the hyperparameters in the workflow.

To accommodate the inherent noise and variability within biological datasets, we also applied a series of convolution iterations to the target volume, and capture each smoothing as a separate volume. This iterative convolutional smoothing leads to an array of volumes and we use each of these volumes in the fitting process. This **multi-resolution approach** enhances the robustness of the fitting process by mitigating the impact of noise and data irregularities. We empirically found that a 10-element array of increasingly smoothed volumes, iteratively filtered with a Gaussian smoothing kernel, performs well. We expose this array’s size as a hyperparameter to allow users to control it. We experimented with Laplacian smoothing as well, which led to unsatisfactory performance. We denote the non-smoothed volume as  $\hat{V}_F^{G_0}$  and express the recurrent formulation of the iterative convolution smoothing as:

$$\hat{V}_F^{G_n} = \hat{V}_F^{G_{n-1}} * G_n$$

A third adaptation we apply to the initial fitting process is a stricter penalization of a mismatch. If an atom center is placed within the cryo-EM map volume but outside the extent of the molecular target structure, i.e., outside of the target *footprint*, where normally the target density would be zero. To discourage such misalignment even more, we assign these regions a **negative value**. After smoothing, therefore, for those voxels with a density value of zero, we replace the zero with a negative value. We experimented with varying the negative values or creating a smooth gradient of negative values but found a constant value of  $-0.5$  outside the molecular footprint within the map performs well. We expose this value, however, as a tunable hyperparameter. We denote the resulting volume as  $\hat{V}_{F_{-c}}^{G_n}$  with  $-c$  being the negative constant value. Finally, we update the loss function formulation with a volume smoothed after  $j$  iterations as:

$$L(\mathbf{p}, \mathbf{q}, \mathbf{X}_m, \hat{V}_{F_{-c}}^{G_j})$$

We weigh each fit with a multi-resolution volume array element  $w_j$  for a total number of resolutions  $n$ , and sum up all the multi-resolution components to form the final loss function for one  $\mathbf{p}$  and  $\mathbf{q}$  pair:

$$L_m([p, q]) = \sum_{j=1}^n w_j \cdot L(\mathbf{p}, \mathbf{q}, \mathbf{X}_m, \hat{V}_{F_{-c}}^{G_j}) \quad (6)$$

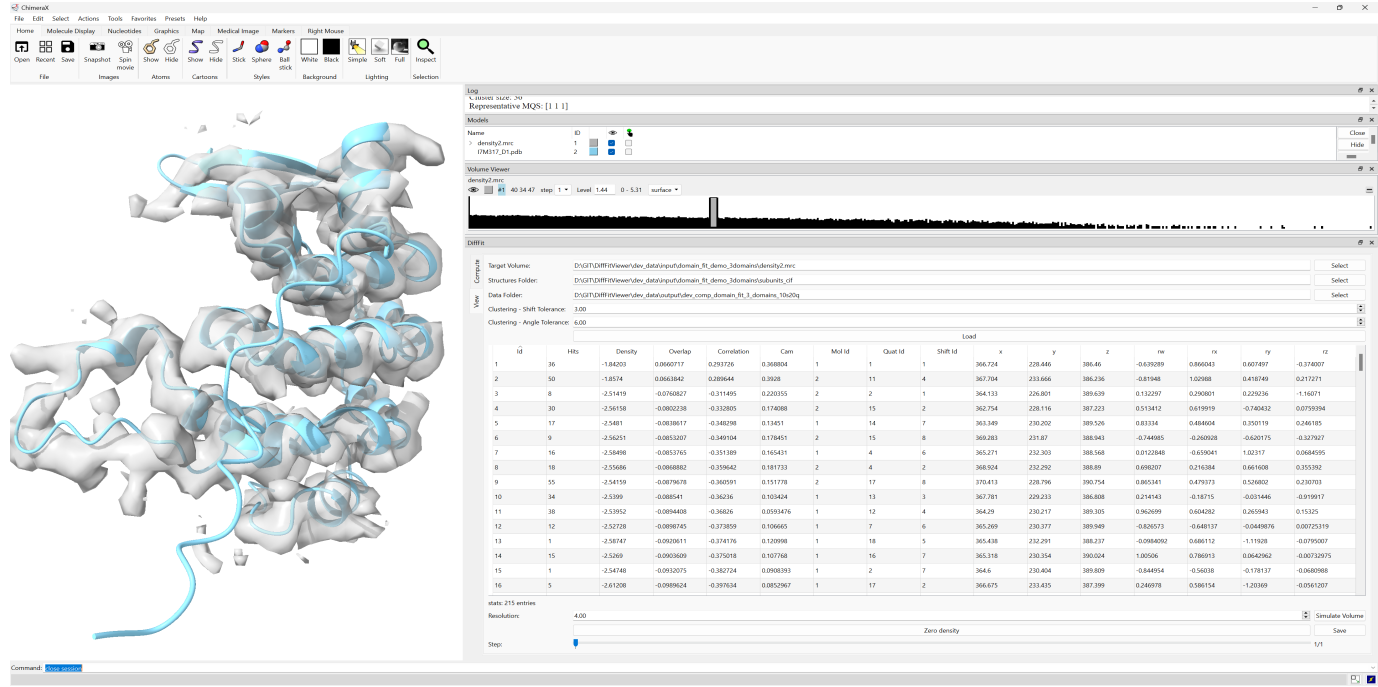


Fig. 4: Our visual browser based on ChimeraX. The target volume in the left is overlaid with a fitted molecule corresponding to the selected fit result in the table on the right (clustered fits, each row being the representative placement with the highest correlation from that cluster). After inspection, users can save the placement and then select “Simulate volume” and “Zero density” to zero out the corresponding voxels from the target volume.

To start the optimization we need to initialize the position offset  $\mathbf{p}$  and the rotation quaternion  $\mathbf{q}$ . We uniformly sample  $N_{\mathbf{q}}$  points on a unit sphere and then convert these into quaternions to be applied for each offset position. Instead of uniformly sampling positions from the volume’s bounding box (as in ChimeraX), we uniformly sample  $N_{\mathbf{p}}$  positions from the positive voxels in the filtered and normalized volume  $\hat{V}_{F_c}$ . This **data-adaptive initialization** increases our success rate by a factor of two by searching from  $N_{\mathbf{q}} \cdot N_{\mathbf{p}}$  initial placements, as compared to ChimeraX’ traditional initialization.

### 3.1.4 Fitting multiple placements of one molecule

To look for fits for multiple copies of a single molecule  $m$ , we then take advantage of GPU parallelization and optimize all  $N_{\mathbf{q}} \cdot N_{\mathbf{p}}$  pairs of  $[\mathbf{p}, \mathbf{q}]$  of the molecule with atoms  $\mathbf{X}_m$  altogether in one single loss function:

$$L_{par}(m) = \sum_{k=1}^{N_{\mathbf{q}} \cdot N_{\mathbf{p}}} L_m([\mathbf{p}_k, \mathbf{q}_k]). \quad (7)$$

### 3.1.5 Fitting multiple placements of multiple molecules

Finally, as all subunit molecules have different numbers of atoms, it is not easy to parallelize the treatment of multiple molecules without overhead on the array padding of zeros. And because, usually, the  $N_{\mathbf{q}} \cdot N_{\mathbf{p}}$  initial placements of  $\mathbf{X}_m$  atoms would result in a total number of sampling operations higher than the total number of GPU threads, we process different subunits molecules sequentially in a **for** loop and form an overall loss function for  $M$  molecules as

$$L_{all} = \sum_{l=1}^M L_{par}(l) \quad (8)$$

### 3.1.6 Quantify the fit quality

By sampling in the simulated volume from the molecule, we can get a weight for each atom coordinate as  $W(\mathbf{x}) = S(\mathbf{x}, V_{sim})$ . Then, for all the atoms in a molecule, we can form two vectors, one as sampled density vector  $\mathbf{D} = [D(\mathbf{x}_1), D(\mathbf{x}_2), \dots, D(\mathbf{x}_N)]$  from the target volume, the other as weight vector  $\mathbf{W} = [W(\mathbf{x}_1), W(\mathbf{x}_2), \dots, W(\mathbf{x}_N)]$  from the simulated volume. We can then calculate three alignment metrics, mean overlap

$\mu$ , correlation  $\rho$ , and correlation about the mean  $\rho_{\mu}$  as

$$\mu = \frac{\mathbf{D} \cdot \mathbf{W}}{N}$$

$$\rho = \frac{\mathbf{D} \cdot \mathbf{W}}{|\mathbf{D}| |\mathbf{W}|}$$

$$\rho_{\mu} = \frac{(\mathbf{D} - D_{\mu}) \cdot (\mathbf{W} - W_{\mu})}{|\mathbf{D} - D_{\mu}| |\mathbf{W} - W_{\mu}|}$$

where the subtraction operator represents subtracting the scalar average densities  $D_{\mu}$  and  $W_{\mu}$  from each component of the sampled density vectors. We use these quality metrics during the interactive assessment by the bioscientist in ChimeraX that we describe next.

### 3.2 Visually-guided fitting

A critical aspect of the post-processing of DiffFit involves the clustering and sorting of fitting results to facilitate user-guided selection and refinement. After the optimization phase, the algorithm generates a vast array of potential fits, characterized by their translation and rotation parameters. To manage this abundance of data and facilitate efficient result exploration, we apply a clustering algorithm to group the fitting results based on their spatial and orientational similarity (Fig. 3(c), (e)).

Each cluster represents a set of fits that are closely related, suggesting a consensus among them regarding the position and orientation of the fitted structure within the target volume. We sort these clusters based on a defined metric, such as the overall density overlap or correlation coefficient we just discussed, ensuring that the most promising fits are prioritized for user review. This hierarchical organization allows researchers to quickly identify the most accurate and relevant fitting results, streamlining the analysis process.

To further assist in the exploration of fitting results, we created an interactive visual browser as a comprehensive visualization tool that presents the sorted clusters in a user-friendly format (Fig. 4). This browser displays key metrics for each cluster, including the average correlation coefficient, density overlap, and a consensus error measure, providing a quick overview of each cluster’s quality and relevance. The

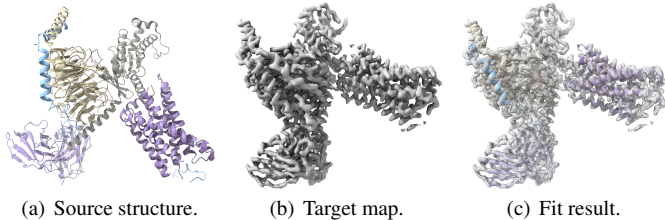


Fig. 5: Fitting a single structure for 8JGF [12].

browser also allows users to select a cluster and visually inspect the fitting results within the 3D context of the target volume. This interactive exploration is crucial for assessing the fit quality in complex cryo-EM map regions, where subtle differences in position or orientation can substantially impact the biological interpretation of the results.

An innovative feature of our approach is the ability to iteratively refine the fitting process through the selective exclusion of already placed molecules' densities. Once a cluster is selected and its fit (or multiple fits) is verified as accurate by the bioscientist, the corresponding density within the target volume can be *zeroed-out*, effectively removing the respective volume region from further consideration in the following part of the fitting process. This step is crucial for complex volumes containing multiple closely situated structures, as it prevents the algorithm from repeatedly fitting structures to the same volume region and reduces false positives when fitting the remaining region.

Thus by iteratively fitting and zeroing out densities, users can progressively shrink the target volume, isolating and identifying individual structures within a dense or complex dataset. This iterative refinement approach ensures that the fitting process is not only guided by the algorithm's optimization but also by the user's expert knowledge and visual assessment, ultimately leading to more accurate and biologically meaningful results.

Our resulting visually-guided fitting framework enhances the DiffFit algorithm by integrating clustering, sorting, and interactive exploration tools. These features enable users to efficiently filter through large datasets of fitting results, identify the most promising fits, and iteratively refine the fitting process based on visual assessment. The combination of automated optimization with user-guided inspection and filtering addresses the challenge of accurately fitting molecular subunit structures within volumetric data.

## 4 IMPLEMENTATION

We utilized PyTorch for the DiffFit algorithm implementation, capitalizing on its dynamic computational graph, automatic differentiation, and GPU acceleration to estimate positional offset and rotational quaternion parameters efficiently. Specifically, we employed `torch.nn.Conv3d` for Gaussian smoothing and `torch.nn.functional.grid_sample` for trilinear interpolation with padding mode set to "border." This approach enables rapid processing of large volumes and multiple structures. We leveraged tensor operations and the Adam optimization algorithm for accurate optimization results. We also integrated additional functions from SciPy, Bio.PDB, mrcfile, and Numpy libraries to enhance the algorithm's functionality. In addition, DiffFit was seamlessly integrated into ChimeraX (Fig. 4), based on its bundle development environment.

## 5 USE CASE SCENARIOS

We designed DiffFit, with its advanced fitting algorithms and integration with visualization tools, to tackle a range of challenges in structural biology. We thus now explore three key scenarios where DiffFit can be particularly impactful, demonstrating its versatility and potential.

### 5.1 Scenario 1: Fit a single structure

The most straightforward application of DiffFit is the fitting of a single atomistic structure into a target volumetric map, for which we show an example in Fig. 5. This scenario is common in cases where an already resolved protein structure or a predicted structure needs to be placed

Table 1: Performance results of fitting a single structure.

Structure	C Hit	D Hit	Gain	C Time	D Time	Gain
8JGF [12]	11	380	35x	0:38:57	0:00:12	195x
8X79 [48]	1	292	292x	0:30:33	0:00:14	131x
8GAM [16]	3	396	132x	1:31:37	0:00:14	393x

C stands for ChimeraX, D stands for DiffFit; Gain = D/C for Hit and C/D for Time.

within a newly reconstructed volume captured through cryo-EM for further refinement.

In this scenario, DiffFit's optimization efficiently determines the optimal position and orientation of the protein (Fig. 5(a)) within the volume (Fig. 5(b)). The whole fitting process is automatic, removing the prerequisite of manually placing the structure at an approximate orientation close to the final optimal. The interactive visually-guided inspection process allows researchers to verify the fit (Fig. 5(c)), leveraging their expertise to ensure biological relevance and accuracy. We report the successful hit rate and computation times in Table 1 and compare them with the current solution in ChimeraX for four recently published structures, for which we fitted each structure 1000 times to obtain reliable results. The reported performance values are based on a workstation that uses a Nvidia RTX 4090 GPU for the DiffFit part, and single thread on an AMD Ryzen Threadripper PRO 3995WX 2.70 GHz for the ChimeraX fitmap command.

### 5.2 Scenario 2: Composite multiple structures

A more complex use case involves the fitting of multiple structures into a single, large, often complex, volumetric dataset, such as assembling a viral capsid from individual protein units or constructing a ribosomal complex from its constituent proteins and RNA molecules. DiffFit can handle such composite fitting tasks by iteratively optimizing the placement of each component, from biggest to smallest, while considering the spatial relationships and interactions among them to prevent overlaps and ensure a coherent assembly.

Fig. 1 shows an example of compositing multiple structures into a cryo-EM volume map, for the PDB-protein 8SMK [53]. In the first row we show how the middle and bottom parts are fitted in a first round of computation, with the remaining top part of the protein being fitted in a second round of our interactive process.

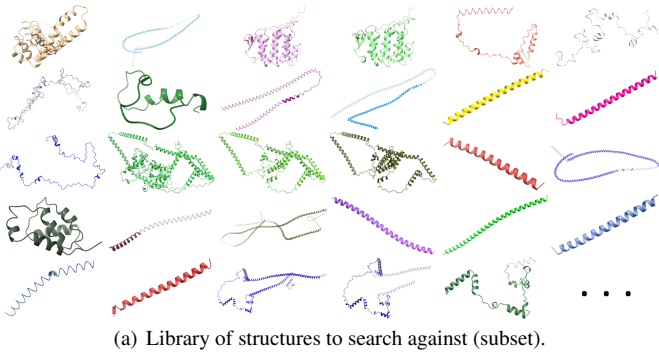
The ability to *zero-out* densities, once a fit is confirmed, allows DiffFit to sequentially fit multiple structures without interference from previously placed components, as we demonstrate in Fig. 1. This iterative approach is particularly useful for densely packed molecular complexes where individual components may be difficult to distinguish in the volumetric data. This scenario is critical for understanding the functional context of proteins within larger biomolecular assemblies or cellular environments.

### 5.3 Scenario 3: Identify unknown densities

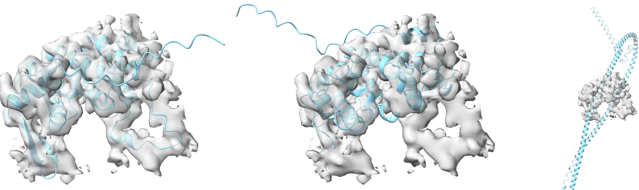
DiffFit also offers bioscientists the capability to identify and characterize unknown densities within volumetric datasets. In cases where a volume contains unassigned or ambiguous regions, possibly indicating the presence of previously unidentified molecules or molecular complexes, DiffFit can be used to screen a library of known structures and predicted structures for potential matches.

By fitting the structures from a library into the unidentified densities and evaluating the fit quality, researchers can hypothesize the identity of the unknown components. This scenario is invaluable for discovery-based research, where identifying novel components within complex molecular assemblies can lead to significant biological insights.

We performed the search with the demo dataset from a recent automated domain-level protein identification technique, DomainFit [9]. The task is to identify, from a library of 359 protein domains (Fig. 6(a) shows a subset), which one(s) best fits into the given volume (Fig. 6(b)). DomainFit identified two candidates (I7MLV6\_D3, and I7M317\_D1) after first fitting all domains using ChimeraX's `fitmap` command and then performing statistical analyses to remove false positives. With our DiffFit we identified these same two candidates with our fitting



(a) Library of structures to search against (subset).



(b) Unknown density identification; comparison of three potential fits which are overlaid on top of the target volumes.

Fig. 6: Unknown density identification, where dozens to hundreds of molecular structures can be evaluated for potential fit.

Table 2: Performance results of identifying unknown structures.

Structure	C Hit	D Hit	Gain
I7MLV6_D3	108	280	2.6x
I7M317_D1	127	163	1.3x

C stands for ChimeraX, D stands for DiffFit; Gain = D/C for Hit.

technique followed by visual inspection, where the two candidates were the first to be inspected. For the comparison of both approaches we report the hit times the same way as before in Table 2, showing a  $\approx 2\times$  gain on the hit rate. In addition, DomainFit takes approx. 12 hours to finish the task, while with DiffFit it takes  $\approx 10$  minutes—a  $72\times$  gain in computation time.

## 6 FEEDBACK

In addition to quantitative metrics reported in the use-cases above, qualitative feedback from users plays a crucial role in evaluating DiffFit’s practical utility and user experience. We thus solicited feedback from a diverse group of users, including Ph.D. students, structural biologists, and computational scientists, through surveys, interviews, and hands-on testing sessions. In total, 7 people responded to our request, and we report key themes from their qualitative feedback as follows.

**Usability.** Our participants appreciated DiffFit’s intuitive interface and workflow (“quite intuitive and easy to use”), which significantly lowers the barrier to entry for new users, while still providing advanced features for experienced researchers. The visually-guided fitting process, in particular, was highlighted as a powerful feature for refining fitting results based on expert judgment. Suggestions for further improving this interaction step were to show several visual clusters at a time, to be able to visually compare the fits, and some tabbing-based way to check the various clusters. This would make it easier to observe how each cluster fits relative to the cryo-EM volume and thus researchers would be better able to focus on a particular chain of interest.

**Impact on Research.** The participants reported that DiffFit has the potential to have a tangible impact on their research, enabling them to tackle complex fitting challenges that were previously out of reach, such as the ability to rapidly sample a large database of candidate structures for regions with unassigned protein density. The new ability to rapidly and accurately fit structures into volumetric data opens up new avenues of investigation and has the potential to accelerate discoveries in structural biology and one respondent stated that our automatic fitting

and visual inspection approach “could be a key feature in ChimeraX that [could become] a standard in many pipelines” as well as “a key implementation [for] a standard modeling workflow.”

The respondents also added suggestions for future development, such as a better structuring of the handling of the associated files and the addition of workflows that would rely on automatically creating model subdivisions and doing fits on those, before integrating the results into the reference volume. They also highlighted further potential such as using our approach for the analysis of density maps that are generated through X-ray crystallography.

## 7 LIMITATIONS AND FUTURE WORK

While we report substantial improvements over the state-of-the-art techniques, our technique also has its limitations. One issue arises in Scenario 2, due to the gradual *zeroing-out* the target map, when we composite multiple structures into a single map. In this case the volume removal can potentially remove some voxels that are also part of adjacent interacting molecular subunits. The next to-be-fitted subunit might then have difficulties to find its correct location as these few zeroed voxels penalize its correct position. We are in the process of investigating this limitation in the future and plan to experiment with heuristics that remove only those voxels that are fully covered by the molecular structure or to slightly shrink the to-be-zeroed-out region before its removal from the map. Another related limitation is that our fitting process does not check for collisions within adjacent subunits, as previously investigated in visualization work (e.g., [36]). While the map shrinking process should address this issue, in some cases subunits may still end up overlapping. Resolving this issue would be rather straightforward by removing those subunit poses which overlap with previously confirmed subunit placements or perform a minimal pose modification to resolve the structural collision.

Our technique is also not entirely parameter-free, which would be the ideal scenario. The threshold value for removal of voxels with small density values, for example, and the threshold value for the connected-voxel minimal cluster size need to be set manually. Manipulating these parameters requires prior domain experience with cryo-EM data from the bioscientists. We plan to automate identification of these thresholds or, at least, define suitable default values and provide guidance about reasonable parameter ranges.

The visualization design in our current version of the tool also offers only the most essential visual encoding types, with a clear potential for further improvement. We plan to adapt comparative visualization techniques for intersecting surfaces and smart visibility techniques for combined rendering of volumetric density representation with molecular surfaces or cartoon representations. Furthermore, visualization design for analyzing the structural poses within a cluster suffers from high spatial occlusion among the subunits’ various poses (see Fig. 3(d)). This is a common domain problem and a dedicated research effort will be needed to combat the occlusion of this magnitude.

Driven by the feedback we received, additional possible future directions include extending DiffFit to deformable transformations, take stoichiometry and symmetry into consideration, and speeding up it by integration with CUDA.

## 8 CONCLUSION

In conclusion, DiffFit offers a novel and efficient solution to the challenges of atom-to-map fitting that has recently arisen in structural biology. We address these challenges with our differentiable fitting algorithm along with a set of essential strategies that make the algorithm robust for the domain problem, adding a human-in-the-loop visual analytics approach to the workflow, and providing our approach as an open-source package that is designed to work as part of a standard software tool of the domain (ChimeraX). A key ingredient to our approach was the change from pixel-to-pixel (or the equivalent voxel-to-voxel) fitting to points-to-volume fitting, which enabled us to deal with the specific constraints of the fitting problem in structural biology. In hindsight, as we witness the success of using atom coordinates to sample the volume instead of using all the voxels, DiffFit suggests that, in Reddy’s [35] original technique that inspired our work, maybe not all

the pixels in a patch are needed for the optimization, which means that the image compositing optimization could be more efficient and could handle larger examples with faster processing.

The quantitative performance metrics we reported collectively demonstrate DiffFit's substantial improvement over traditional approaches, highlighting its potential to transform the field of structural biology. This potential is particularly large because the workflows of Assembleline, a protocol published in 2022 [34], and DomainFit [9], so far, rely on ChimeraX's `fitmap` command as their first step. This stage can now be replaced by our more effective DiffFit, laying a new foundation for these and other workflows. By demonstrating the effectiveness of our technique across three scenarios, from fitting individual structures to assembling complex molecular architectures and identifying unknown components, we demonstrated that DiffFit overcomes the limitations of manually placing individual molecules before fitting, makes the compositing faster, more accurate, and intuitive, and opens the possibility of scanning the whole set of known and predicted molecules with the current computational resources. Ultimately, we thus escape the **Faustian bargain** [46] and instead are now free ourselves to explore the inner workings of the biological world.

## ACKNOWLEDGMENTS

This research was supported by King Abdullah University of Science and Technology (KAUST) (BAS/1/1680-01-01).

## SUPPLEMENTAL MATERIAL POINTERS

We provide the open-source repository of our tool at [github.com/nanovis/DiffFitViewer](https://github.com/nanovis/DiffFitViewer). Other supplemental material is available at [osf.io/5tx4q](https://osf.io/5tx4q).

## IMAGES LICENSE AND COPYRIGHT

We as authors state that all of our figures are and remain under our own personal copyright, with the permission to be used here. We also make them available under the [Creative Commons Attribution 4.0 International \(@ CC BY 4.0\)](#) license and share them at [osf.io/5tx4q](https://osf.io/5tx4q).

## REFERENCES

- [1] P. Arora, R. Mehta, and R. Ahuja. An integration of meta-heuristic approach utilizing kernel principal component analysis for multimodal medical image registration. *Cluster Comput.*, 24 pages, 2024. To appear. doi: [10/gtmxvd](https://doi.org/10/gtmxvd)
- [2] X.-c. Bai, G. McMullan, and S. H. W. Scheres. How cryo-EM is revolutionizing structural biology. *Trends Biochem Sci.*, 40(1):49–57, 2015. doi: [10/f6wq7v](https://doi.org/10/f6wq7v)
- [3] W. Chen, X. Wang, and Y. Wang. FFF: Fragment-guided flexible fitting for building complete protein structures. In *Proc. CVPR*, pp. 19776–19785. IEEE CS, Los Alamitos, 2023. doi: [10/gtmxvf](https://doi.org/10/gtmxvf)
- [4] J. P. Didon and F. Langevin. Registration of MR images: From 2D to 3D, using a projection based cross correlation method. In *Proc. EMBC*, vol. 1, pp. 489–490. IEEE, Piscataway, 1995. doi: [10/bgp7mt](https://doi.org/10/bgp7mt)
- [5] D. Duran, P. Hermosilla, T. Ropinski, B. Kozlíková, Á. Vinacua, and P.-P. Vázquez. Visualization of large molecular trajectories. *IEEE Trans Vis Comput Graph*, 25(1):987–996, 2019. doi: [10/gjbdnk](https://doi.org/10/gjbdnk)
- [6] M. Falk, V. Tobiasson, A. Bock, C. Hansen, and A. Ynnerman. A visual environment for data driven protein modeling and validation. *IEEE Trans Vis Comput Graph*, 11 pages, 2024. To appear. doi: [10/gsc3c9](https://doi.org/10/gsc3c9)
- [7] B. Frenz, A. C. Walls, E. H. Egelman, D. Veesler, and F. DiMaio. RosettaES: A sampling strategy enabling automated interpretation of difficult cryo-EM maps. *Nat. Methods*, 14(8):797–800, 2017. doi: [10/gf5cmq](https://doi.org/10/gf5cmq)
- [8] Y. Fu, Y. Lei, T. Wang, W. J. Curran, T. Liu, and X. Yang. Deep learning in medical image registration: A review. *Phys Med Biol.*, 65(20), article no. 20TR01, 27 pages, 2020. doi: [10/ghn45h](https://doi.org/10/ghn45h)
- [9] J. Gao, M. Tong, C. Lee, J. Gaertig, T. Legal, and K. H. Bui. DomainFit: Identification of protein domains in cryo-EM maps at intermediate resolution using AlphaFold2-predicted models. bioRxiv preprint 2023.11.28.569001, 2023. doi: [10/gs63f2](https://doi.org/10/gs63f2)
- [10] J. I. Garzón, J. Kovacs, R. Abagyan, and P. Chacón. ADP\_EM: Fast exhaustive multi-resolution docking for high-throughput coverage. *Bioinf.*, 23(4):427–433, 2006. doi: [10/c9xkmg](https://doi.org/10/c9xkmg)
- [11] T. D. Goddard, C. C. Huang, and T. E. Ferrin. Visualizing density maps with UCSF Chimera. *J Struct Biol.*, 157(1):281–287, 2007. Software tools for macromolecular microscopy. doi: [10/fi849s](https://doi.org/10/fi849s)
- [12] L. Guo, Y. Zhang, G. Fang, L. Tie, Y. Zhuang, C. Xue, Q. Liu, M. Zhang, K. Zhu, C. You, P. Xu, Q. Yuan, C. Zhang, L. Liu, N. Rong, S. Peng, Y. Liu, C. Wang, X. Luo, Z. Lv, D. Kang, X. Yu, C. Zhang, Y. Jiang, X. Dong, J. Zhou, Z. Liu, F. Yang, H. E. Xu, and J.-P. Sun. Ligand recognition and G protein coupling of the human itch receptor MRGPRX1. *Nat Commun.*, 14, article no. 5004, 12 pages, 2023. doi: [10/mpt4](https://doi.org/10/mpt4)
- [13] B. He, F. Zhang, C. Feng, J. Yang, X. Gao, and R. Han. Accurate global and local 3D alignment of cryo-EM density maps using local spatial structural features. *Nat Commun.*, 15, article no. 1593, 15 pages, 2024. doi: [10/gtmxvg](https://doi.org/10/gtmxvg)
- [14] M. A. Herzik, M. Wu, and G. C. Lander. High-resolution structure determination of sub-100 kDa complexes using conventional cryo-EM. *Nat Commun.*, 10, article no. 1032, 9 pages, 2019. doi: [10/gg7zp4](https://doi.org/10/gg7zp4)
- [15] D. L. G. Hill, P. G. Batchelor, M. Holden, and D. J. Hawkes. Medical image registration. *Phys Med Biol.*, 46(3):R1–R45, 2001. doi: [10/fgbhgj](https://doi.org/10/fgbhgj)
- [16] C. Hu, M. T. Myers, X. Zhou, Z. Hou, M. L. Lozen, K. H. Nam, Y. Zhang, and A. Ke. Exploiting activation and inactivation mechanisms in type I-C CRISPR-Cas3 for genome-editing applications. *Mol Cell*, 84(3):463–475, 2024. doi: [10/mpt7](https://doi.org/10/mpt7)
- [17] J. Jumper, R. Evans, A. Pritzel, T. Green, M. Figurnov, O. Ronneberger, K. Tunyasuvunakool, R. Bates, A. Žídek, A. Potapenko, A. Bridgland, C. Meyer, S. A. A. Kohl, A. J. Ballard, A. Cowie, B. Romera-Paredes, S. Nikolov, R. Jain, J. Adler, T. Back, S. Petersen, D. Reiman, E. Clancy, M. Zielinski, M. Steinegger, M. Pacholska, T. Berghammer, S. Bodenstein, D. Silver, O. Vinyals, A. W. Senior, K. Kavukcuoglu, P. Kohli, and D. Hassabis. Highly accurate protein structure prediction with AlphaFold. *Nature*, 596:583–589, 2021. doi: [10/gk7nfp](https://doi.org/10/gk7nfp)
- [18] M. Kesäniemi and K. Virtanen. Direct least square fitting of hyperellipsoids. *IEEE Trans Pattern Anal Mach Intell.*, 40(1):63–76, 2018. doi: [10/gcqjrb](https://doi.org/10/gcqjrb)
- [19] D. P. Kingma and J. Ba. Adam: A method for stochastic optimization. arXiv preprint 1412.6980, 2017. doi: [10/hnk](https://doi.org/10/hnk)
- [20] S. Klein, J. P. W. Pluim, M. Staring, and M. A. Viergever. Adaptive stochastic gradient descent optimisation for image registration. *Int J Comput Vis.*, 81(3):227–239, 2009. doi: [10/dghjcp](https://doi.org/10/dghjcp)
- [21] Y.-B. Kou, Y.-F. Feng, L.-Y. Shen, X. Li, and C.-M. Yuan. Adaptive spline surface fitting with arbitrary topological control mesh. *IEEE Trans Vis Comput Graph*, 13 pages, 2024. To appear. doi: [10/gtmxw4](https://doi.org/10/gtmxw4)
- [22] D. Kućák, M. N. Selzer, J. Byška, M. L. Ganuza, I. Baršiš, B. Kozlíková, and H. Miao. Vivern—A virtual environment for multiscale visualization and modeling of DNA nanostructures. *IEEE Trans Vis Comput Graph*, 28(12):4825–4838, 2022. doi: [10/mpwt](https://doi.org/10/mpwt)
- [23] K. Lasker, O. Dror, M. Shatsky, R. Nussinov, and H. J. Wolfson. EMatch: Discovery of high resolution structural homologues of protein domains in intermediate resolution cryo-EM maps. *IEEE/ACM Trans Comput Biol Bioinf.*, 4(1):28–39, 2007. doi: [10/ccbr4m](https://doi.org/10/ccbr4m)
- [24] D. Lowe. Distinctive image features from scale-invariant keypoints. *Int J Comput Vision*, 60(2):91–110, 2004. doi: [10/bqrmsp](https://doi.org/10/bqrmsp)
- [25] S. Malhotra, S. Träger, M. Dal Peraro, and M. Topf. Modelling structures in cryo-EM maps. *Curr Opin Struct Biol.*, 58:105–114, 2019. doi: [10/gtmxve](https://doi.org/10/gtmxve)
- [26] M. Malinsky, R. Peter, E. Hodneland, A. J. Lundervold, A. Lundervold, and J. Jan. Registration of FA and T1-weighted MRI data of healthy human brain based on template matching and normalized cross-correlation. *J Digit Imaging*, 26(4):774–785, 2013. doi: [10/gtmxw5](https://doi.org/10/gtmxw5)
- [27] V. Mallet, C. Rapisarda, H. Minoux, and M. Ovsjanikov. Finding antibodies in cryo-EM densities with CrAI. bioRxiv preprint 2023.09.27.559736, 2023. doi: [10/gtn9kj](https://doi.org/10/gtn9kj)
- [28] D. Mattes, D. R. Haynor, H. Vesselle, T. K. Lewellen, and W. Eubank. PET-CT image registration in the chest using free-form deformations. *IEEE Trans Med Imaging*, 22(1):120–128, 2003. doi: [10/cs4pch](https://doi.org/10/cs4pch)
- [29] T. Nakane, A. Kotecha, A. Sente, G. J. McMullan, S. Masiulis, P. M. G. E. Brown, I. Grigoras, L. Malinauskaitė, T. Malinauskas, J. Miehling, L. Yu, D. Karia, E. V. Pechnikova, E. de Jong, J. Keizer, M. Bischoff, J. McCormack, P. Tiemeijer, S. W. Hardwick, D. Y. Chirgadze, G. N. Murshudov, A. R. Aricescu, and S. H. W. Scheres. Single-particle cryo-EM at atomic resolution. *Nature*, 587(7832):152–156, 2020. doi: [10/gwcfp](https://doi.org/10/gwcfp)
- [30] N. Nguyen, O. Strnad, T. Klein, D. Luo, R. Alharbi, P. Wonka, M. Maritan, P. Mindek, L. Autin, D. S. Goodsell, and I. Viola. Modeling in the time of COVID-19: Statistical and rule-based mesoscale models. *IEEE Trans Vis*

- Comput Graph*, 27(2):722–732, 2021. doi: [10/k8sh](#)
- [31] E. F. Pettersen, T. D. Goddard, C. C. Huang, G. S. Couch, D. M. Greenblatt, E. C. Meng, and T. E. Ferrin. UCSF Chimera—A visualization system for exploratory research and analysis. *J Comput Chem*, 25(13):1605–1612, 2004. doi: [10/b4bq4c](#)
- [32] J. Pfab, P. Minh Nhut, and D. Si. DeepTracer for fast de novo cryo-EM protein structure modeling and special studies on CoV-related complexes. *PNAS*, 118(2), article no. e2017525118, 12 pages, 2021. doi: [10/gjnkwt](#)
- [33] J. P. W. Pluim, J. B. A. Maintz, and M. A. Viergever. Mutual-information-based registration of medical images: A survey. *IEEE Trans. Med. Imaging*, 22(8):986–1004, 2003. doi: [10/czrq8h](#)
- [34] V. Rantos, K. Karius, and J. Kosinski. Integrative structural modeling of macromolecular complexes using Assembleline. *Nat Protoc*, 17:152–176, 2022. doi: [10/gq586q](#)
- [35] P. Reddy, P. Guerrero, M. Fisher, W. Li, and N. J. Mitra. Discovering pattern structure using differentiable compositing. *ACM Trans Graph*, 39(6), article no. 262, 15 pages, 2020. doi: [10/gtmxvb](#)
- [36] J. Schmidt, R. Preiner, T. Auzinger, M. Wimmer, M. E. Gröller, and S. Bruckner. YMCA – Your mesh comparison application. In *Proc. VAST*, pp. 153–162. IEEE CS, Los Alamitos, 2014. doi: [10/f3sttr](#)
- [37] M. Schäfer, N. Brich, J. Byška, S. M. Marques, D. Bednář, P. Thiel, B. Kožlíková, and M. Krone. InVADo: Interactive visual analysis of molecular docking data. *IEEE Trans Vis Comput Graph*, 30(4):1984–1997, 2024. doi: [10/gtnn2n](#)
- [38] A. Seiler, D. Großmann, and B. Jüttler. Spline surface fitting using normal data and norm-like functions. *Comput Aided Geom Des*, 64:37–49, 2018. doi: [10/gd5gt4](#)
- [39] T. R. Shamam, T. Dekel, and T. Michaeli. SinGAN: Learning a generative model from a single natural image. In *Proc. ICCV*, pp. 4569–4579. IEEE CS, Los Alamitos, 2019. doi: [10/gg8fc3](#)
- [40] L. Shang, J. Lv, and Z. Yi. Rigid medical image registration using PCA neural network. *Neurocomput*, 69(13–15):1717–1722, 2006. doi: [10/fsrrb2](#)
- [41] R. Skånsberg, I. Hotz, A. Ynnerman, and M. Linares. VIAMD: A software for visual interactive analysis of molecular dynamics. *J Chem Inf Model*, 63(23):7382–7391, 2023. doi: [10/gs7tzh](#)
- [42] R. Skånsberg, P.-P. Vázquez, V. Guallar, and T. Ropinski. Real-time molecular visualization supporting diffuse interreflections and ambient occlusion. *IEEE Trans Vis Comput Graph*, 22(1):718–727, 2016. doi: [10/mpwv](#)
- [43] T. Terwilliger, P. Adams, P. Afonine, and O. Sobolev. A fully automatic method yielding initial models from high-resolution cryo-electron microscopy maps. *Nat Methods*, 15(11):905–908, 2018. doi: [10/gfnb8d](#)
- [44] P. Thevenaz and M. Unser. Optimization of mutual information for multiresolution image registration. *IEEE Trans Image Process*, 9(12):2083–2099, 2000. doi: [10/fs4j7h](#)
- [45] P. Ulbrich, M. Waldner, K. Furmanová, S. M. Marques, D. Bednář, B. Kožlíková, and J. Byška. sMolBoxes: Dataflow model for molecular dynamics exploration. *IEEE Trans Vis Comput Graph*, 29(1):581–590, 2023. doi: [10/kvjjv](#)
- [46] J. W. von Goethe. *Faust. Eine Tragödie [Faust: A Tragedy]*. J. G. Cotta, Tübingen, 1808. Online: [gutenberg.org/ebooks/21000](http://gutenberg.org/ebooks/21000); English translation: [gutenberg.org/ebooks/3023](http://gutenberg.org/ebooks/3023).
- [47] T. Walton, M. Gui, S. Velkova, M. R. Fassad, R. A. Hirst, E. Haarman, C. O’Callaghan, M. Bottier, T. Burgoyne, H. M. Mitchison, and A. Brown. Axonemal structures reveal mechanoregulatory and disease mechanisms. *Nature*, 618(7965):625–633, 2023. doi: [10/gscb95](#)
- [48] J. J. Wang, S. Jin, H. Zhang, Y. Xu, W. Hu, Y. Jiang, C. Chen, D. W. Wang, H. E. Xu, and C. Wu. Molecular recognition and activation of the prostacyclin receptor by anti-pulmonary arterial hypertension drugs. *Sci Adv*, 10(6), article no. eadk5184, 11 pages, 2024. doi: [10/mpt5](#)
- [49] R. Y.-R. Wang, M. Kudryashev, X. Li, E. H. Egelman, M. Basler, Y. Cheng, D. Baker, and F. DiMaio. De novo protein structure determination from near-atomic-resolution cryo-EM maps. *Nat Methods*, 12(4):335–338, 2015. doi: [10/gf5cn8](#)
- [50] X. Wang, E. Alnabati, T. W. Aderinwale, S. R. M. V. Subramaniya, G. Terashi, and D. Kihara. Detecting protein and DNA/RNA structures in cryo-EM maps of intermediate resolution using deep learning. *Nat Commun*, 12, article no. 2302, 9 pages, 2020. doi: [10/gmz55b](#)
- [51] K. Xu, Z. Wang, J. Shi, H. Li, and Q. C. Zhang. A2-Net: Molecular structure estimation from cryo-EM density volumes. *Proc AAAI Conf Artif Intell*, 33(1):1230–1237, 2019. doi: [10/ghkjcf](#)
- [52] I.-C. Yeh, C.-H. Lin, O. Sorkine, and T.-Y. Lee. Template-based 3D model fitting using dual-domain relaxation. *IEEE Trans Vis Comput Graph*, 17(8):1178–1190, 2011. doi: [10/dkbjmd](#)
- [53] X. Zhou, S. Kong, A. Maker, S. G. Remesh, K. K. Leung, K. A. Verba, and J. A. Wells. Antibody discovery identifies regulatory mechanisms of protein arginine deiminase 4. *Nat Chem Biol*, 2024. To appear. doi: [10/mpwf](#)
- [54] Y. Zhou, Z. Zhu, X. Bai, D. Lischinski, D. Cohen-Or, and H. Huang. Non-stationary texture synthesis by adversarial expansion. *ACM Trans Graph*, 37(4), article no. 49, 13 pages, 2018. doi: [10/gd52tv](#)